Publication Year	2021
Acceptance in OA@INAF	2022-11-21T10:04:54Z
Title	Determination of optical constants from Martian analog materials using a spectro-polarimetric technique
Authors	Alemanno, G.; Garcia-Caurel, E.; Carter, J.; Poulet, F.; Brunetto, R.; et al.
DOI	10.1016/j.pss.2020.105138
Handle	http://hdl.handle.net/20.500.12386/32724
Journal	PLANETARY AND SPACE SCIENCE
Number	195

Experimental approach for the determination of optical constants from planetary analog materials using a spectro-polarimetric technique

3 G. Alemanno[1,*], E. Garcia-Caurel[2], J. Carter[1], F. Poulet[1], R. Brunetto[1], A. Alèon-Toppani[1], R. G. Urso[1], O. Mivumbi[1], C. Boukari[3], V. Godard[3]

[1]Universitè Paris-Saclay, CNRS, Institut d'astrophysique spatiale, 91405, Orsay, France

6 [2]LPICM, CNRS, Ecole polytechnique, Institut Polytechnique de Paris, F-91128 Palaiseau Cedex, France

[3]CNRS GEOPS UMR 8148 Bassin et Ressources, Bâtiment 504, Orsay, Cedex, France

9 ## Abstract

We here present our experimental approach to derive optical constants of planetary analogue materials based on an infrared ellipsometry technique. The technique of spectroscopic ellipsometry
12 is a powerful tool for the characterization of the optical properties of materials. This technique represents a significant refinement over the semi-empirical approach to optical constants determination using BRDF (Bidirectional Reflectance Distribution Function) measurements of a
15 finite set of grain sizes for each mineral. It also allows obtaining, not only the optical constants, but also information about the dependence of optical response on sample orientation respect to the illuminating light beam. The ellipsometric technique has been developed more than a century ago,
18 and so far, it is mainly applied to the optical characterization of thin films either for research or for industrial applications. In this work, we show the optical constants for samples of gypsum using data obtained with an infrared spectroscopic Mueller ellipsometer. The set of measurements
21 performed in this work are part of a team effort between the IAS laboratory and the Soleil synchrotron, with the future aim to provide the scientific community with laboratory derived optical constants of different types of materials. Thanks to the high sensitivity of the ellipsometric
24 measurements, and despite of a rather complex data analysis protocol, the results obtained for the gypsum samples show that it is possible to successfully use this technique for direct determination of optical constants of natural minerals. After optimizing the measurement and data analysis
27 protocol will allow to apply the method discussed here to a large number of minerals and materials either natural or man-made.

**Current address:* German Aerospace Center (DLR), Rutherfordstrasse 2, D-12489 Berlin,
30 Germany (giulia.alemanno@dlr.de)

1. Introduction

Optical constants describe the interaction of the matter with the electromagnetic radiation, taking
33 into account the vibrational and electronic transitions for each wavelength. Particulate matter exists in the Earth's atmosphere as well as in the atmospheres of other planetary bodies and in circumstellar clouds. This matter scatters and absorbs both sunlight and superficial thermal
36 radiation. The values of the optical constants are therefore fundamental to correctly describe a variety of physical environments like planetary atmospheres, circumstellar clouds, material abundances on a planet's surfaces and the behavior of satellites' regolith (Marzo et al., 2004).
39 Using remote sensing data, it is, for example, possible to make quantitative estimates of the mineralogical composition on a planet's surface. However, to interpret the spectra acquired from the surface of a planetary body, an appropriate radiative transfer model is necessary that takes into
42 account the combined influence of the atmospheric aerosol and gas, and the surface. Radiative transfer models describe the interaction between surface and atmosphere and allow for a proper determination of the effect of the presence of these particles on the optical measurements acquired
45 from the surface of a planet. However, to do this, such models require a good knowledge of the optical constants for each component that may be present on the area under examination (Poulet et al., 2002; Poulet et al., 2014). Applying these models is difficult in the NIR and MIR due to the
48 absence of optical constants for many important minerals in the monoclinic and triclinic crystal systems.

In particular, in the case of Mars, the increasing quantity of remote sensing data requires a big effort
51 from the scientific community for their interpretation. Thanks to high-resolution mapping using visible and near infrared spectrometers in orbit around the planet, it has been possible to reveal the presence of several and diverse mineral deposits on the Martian surface (Poulet et al., 2005; Bibring
54 et al.; 2006, Ehlmann and Edwards, 2014). However, quantitative analysis within these deposits can allow one to provide important knowledge on the type of process that brought to their origin (allowing to distinguish between depositional and diagenetic mechanism). This information will be
57 essential to constrain the nature of global and local-scale mineralogical transitions on the planet (Stack and Milliken, 2015).

In this work we discuss a method to obtain the optical constants of Martian analogue materials in
60 the mid-far infrared range using spectroscopic Mueller ellipsometry technique, which is an extension of standard ellipsometry. Ellipsometry consists of the use of polarized light to characterize the optical properties of materials, either in bulk or in thin film format. In standard
63 ellipsometry the light beam must remain completely polarized during the whole measurement process (Garcia-Caurel et al., 2015). However, Mueller ellipsometry, being a generalization of

standard ellipsometry, can handle partially polarized light, and therefore it can be used to measure
66 inhomogeneous and/or anisotropic samples if an appropriate model is used to interpret the experimental data which accounts for such non homogeneity. Under the latter assumption, Mueller ellipsometry allows, to properly measure and interpret the properties of partially polarized light
69 (Garcia-Caurel et al., 2015). In the infrared range, the dielectric function is sensitive to vibrational absorptions related to molecular bonds. Therefore, infrared ellipsometry can be used to study chemical composition, crystallinity or doping levels of different types of materials, such as
72 semiconductors, oxides or polymers (Garcia-Caurel et al., 2015).

Spectroscopic Ellipsometry despite of being widely used to the optical characterization of thin films it has been scarcely used to the determination of optical constants of planetary analog materials or
75 similar minerals. The purpose of this paper is to present the use this technique for the optical characterization of materials of Martian interest such as hydrated silicates (like phyllosilicates, hydrated silica) and evaporites (like carbonates, sulfates and chlorides) with the main goal to
78 provide the scientific community with missing data on optical constants on these kinds of materials. The work done so far, aims to put the basis of a facility for optical constants measurements on materials serving as planetary analogues. Here it is discussed the work done to define a
81 measurement protocol and a data modelling procedure that has the potential to be extended and applied to the study of other materials and planetary surfaces. For the sake of illustration, the use of ellipsometry has been applied on a set of gypsum samples. In the following sections, we present the
84 sample preparation procedure (Section 2), the experimental set-up (Section 3) and the measurement protocol and the data modelling and analysis (Section 4). The results obtained are shown in Section 5 along with a comparison with literature. Finally, Section 6 shows a discussion on the overall
87 methodology and on future developments.

2. Sample preparation protocol

To be measured with the Mueller ellipsometer that was used for this particular example (see Fig. 1),
90 samples need to be prepared in a way that makes their surface as polished as possible, keeping also attention to the parallelism of the two sample's surfaces. After several tests, the final sample preparation procedure was defined by the following steps:

93
- **Step 1** – Cutting – The bulk materials are cut in in smaller pieces keeping attention to the parallelism of the two surfaces of the sample;
- **Step 2** – Resin – The pieces obtained from Step 1 are embedded in a mixture of resin (90%) + hardener (10%); 96
- **Step 3** – Oven – Samples from Step 2 are left in an oven at 42°C for almost three hours;

- **Step 4** – Press – An hydraulic press is used to take out the sample from the sample holder;
- **Step 5** – Polish – For each sample prepared six consecutive runs of polishing are performed: - 1) pad used P320 – lubricant water – time: 20 s; 2) pad used P800 – lubricant water – time: 20 s; 3) pad used P1200 – lubricant water – time: 20 s; 4) pad used 3 um – lubricant diamond paste – time: 5 m; 5) pad used 1 um – lubricant diamond paste – time: 5 m; 6) pad used ¼ um – lubricant diamond paste – time: 10 m.
- **Step 6** – Cutting 2 – After polishing, each sample is cut (keeping once again attention to the parallelism of the two surfaces of the polymer) to obtain a thickness of almost 60-70 mm that is adapted for the sample holder of the used instrument. This step can be avoided or modified depending on the sample holder of the instrument to be used.

3. Experimental methodology

3.1 Description of the experimental setup

The experimental setup used for the optical measurements, consists of an in-house broadband Mueller ellipsometer designed to work in the mid-infrared range, from 3 to 14 μm (Garcia-Caurel et al., 2015). The Mueller Ellipsometer is installed at the SOLEIL Synchrotron laboratories and it is composed by a light source, an input arm, an exit arm and an acquisition system. In **Fig. 1**, a schematic representation of the experimental set-up and a picture of it, are shown. The illumination source is a commercial FTIR spectrometer providing an infrared beam in a continuous spectral range from 2.5 to 14 μm. The input arm is a Polarization State Generator (PSG) composed by one fixed grid type linear polarizer and an achromatic retarder mounted in a rotatable holder. The retarder consists of two identical Fresnel rhombs disposed symmetrically and joined in a 'V' shape. A sequentially rotation of the retarder respect to the fixed position of the polarizer allows generating four optimal polarization states. The retardation is induced by the four total internal reflections of the beam during its propagation through the bi-prim. The exit arm is a Polarization State Analyzer (PSA) with the same optical components of the PSG but mounted in reverse order. Both PSG and PSA contain a mobile sample-holder for calibration samples. The PSG generates four different polarization states and the PSA analyze each of these polarization states, after being transformed by the sample, four times. Each analysis is performed orientating the PSA retarder respect to the axis of transmission of the polarizer at a given angle.

Measurements can be performed either in reflection or in transmission; for this work, we have chosen to use the reflection configuration because it is the most sensitive configuration to measure isotropic and anisotropic substrates (Garcia-Caurel et al., 2015).

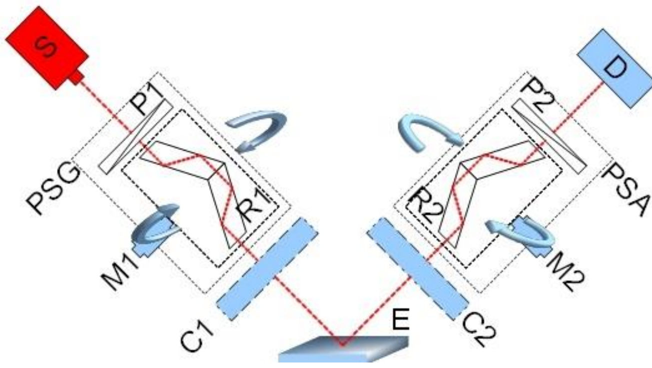

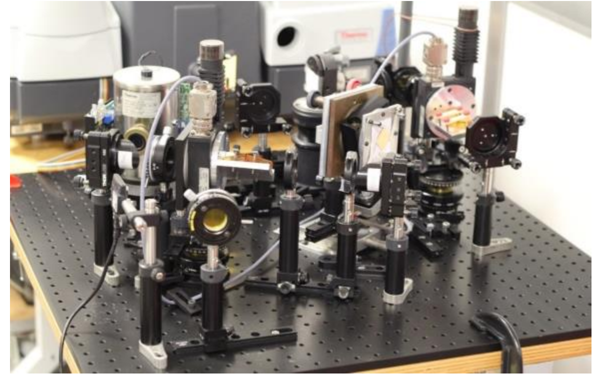

Fig. 1. Left: Schematic representation of a Mueller ellipsometer. Right: picture of the Mueller infrared ellipsometer installed at the SOLEIL laboratories and used for the measurements performed in this project.

The results of an ellipsometric measurement is a set of sixteen independent values that allows calculating the Mueller matrix of the sample (Garcia-Caurel et al., 2015). This matrix is very important because it contains the information about the basic polarimetric effects on the beam light during the measurements. The Mueller matrix of an isotropic sample in reflection can be expressed in terms of the ellipsometric angles Δ and Ψ and it is given by:

$$\mathbf{M}(\tau, \Psi, \Delta) = \tau \begin{pmatrix} 1 & -\cos(2\Psi) & 0 & 0 \\ -\cos(2\Psi) & 1 & 0 & 0 \\ 0 & 0 & \sin(2\Psi)\cos\Delta & -\sin(2\Psi)\sin\Delta \\ 0 & 0 & \sin(2\Psi)\sin\Delta & \sin(2\Psi)\cos\Delta \end{pmatrix} \quad \text{(eq. 1)}$$

where Δ and Ψ measures the change on the polarization state of a beam after reflection or transmission by a sample (Azzam and Bashara 1987). In particular Ψ is related to the change of intensity between the reflected component of the beam light with polarization parallel to the plane of incidence ('p') respect to the one with polarization perpendicular to the plane of incidence ('s'), while Δ measures the phase variation. For an isotropic sample, Δ and Ψ are in turn, related to the Fresnel reflection coefficients through the following relation:

$$\rho = \frac{r_p}{r_s} = \tan\Psi e^{i\Delta} \quad \text{(eq. 2)}$$

where r_p and r_s are the Fresnel reflection coefficient in polarization parallel and perpendicular to the plane of incidence, respectively. The relation reported above, is known as fundamental equation of ellipsometry. From the measured parameters Δ and Ψ, the optical and structural properties of the sample can be determined by appropriate modeling, as we will see in detail in **Section 4**.

3.2 Ellipsometric measurements

153 The prepared gypsum samples have been measured in the MIR range between 2 – 13 μm with a MIR Global Source, a KBr beamsplitter and a MCT detector.

The following procedure has been applied to our samples:

156
- Several test measurements were performed with the aim to properly align the sample respect to the direction of the incident beam light. The number of test measurements done for each sample is not fixed and depends on the time required to find the ‘‘right’’ positions and it increases for anisotropic samples; 159
- Once the sample was properly oriented, the integration time was increased to 32, 64 and even 128 integrations per polarization state, to reduce random noise and therefore to improve the signal to noise ratio. 162

The time required for the measurements increased a lot in the case of anisotropic samples because different azimuthal angles has to be taken into account, as discussed in Section 4.1.1.

165 **3.3 FTIR micro spectral measurements**

In parallel, reflectance measurements were performed with a FTIR Microspectrometer installed at SOLEIL laboratories, to have a comparison standard for the ellipsometric measurements.

168 The FTIR Microspectrometer is a Continuum microscope/ Thermo Nicolet 8700 bench located at the branch line SMIS 2 of the SOLEIL laboratories and it has the following characteristic:

- **Spectral range** covered by an MCT/A detector: 650 - 6000 cm^{-1}, and by an InGaAs detector 2000 - 14000 cm^{-1} 171
- **Spectral resolution**: 0.125 - 32 cm^{-1}
- **Operation modes**: confocal dual aperture, single aperture, reflection and transmission geometry 174
- **Accessories:** Linkam heating stage, microfluidic devices, Thermo ATR accessory
- **Objectives:** 15x (0.58 NA), 32x (0.65 NA), 15x ATR ZnSe

177 The instrument is capable of time resolved studies in Rapid Scan and Step/Scan modes. Samples have been measured at the FTIR Micro-spectrometer in the spectral range 650 - 6000 cm^{-1}. Thanks to the use of the micro-spectrometer, it has been possible to map the surface of the sample and to 180 acquire spectra from different part of the sample surface, in order to evaluate the presence and effect of the inclusions on the average spectra and compare their effect with what we observe in the ellipsometric measurements.

183
4. Data modeling

Ellipsometry is an indirect characterization technique, which in practice means that to extract the optical constants from the measurements a model has to be set up that allows their theoretical
186 calculation. An ellipsometric experiment follows the following procedure:

- An ellipsometric measurement evaluates polarimetric data (ellipsometer angles or Mueller matrices), but not the required parameters like thickness and optical constants;
189
- It is necessary to create a model of the sample to determine the sample parameters;
- Once the model is built, calculated data must be fitted to the experimental data and the best match between the two sets has to be found;
192
- The user has to evaluate the model that "best fits" the experimental data in order to decide if the model is physical reasonable and if the parameters resulting from the fitting routine are quite valid.

195 Once the best fit is obtained, the given model is considered the most sensible representation of reality. Thus, the values for the modeling parameters (like the optical constants) will be considered as the ones representing the real values.
198 The real and imaginary part of the optical properties of solids are wavelength-energy dependent. This dependency can be described by parametric dispersion formulae. The selection of an appropriate model for the optical constant retrieval is in general not direct, and different options
201 may be valid. The choice depends, primarily, on the material and also on the spectral range selected for the analysis (Jellison G.E. 1993). In the infrared spectral range, a constant refractive index (ε_∞) is used to represent the contributions to the dielectric function at frequencies higher than the
204 infrared, and, then, for each clearly visible vibrational mode a Kim oscillator is added. This type of oscillator is an extension of the simple harmonic oscillator model for vibrational modes and it has been suggested by Kim and colleagues (1992). The Kim oscillator allows for a continuous shift of
207 the line shape between a Gaussian and a Lorentzian profile and it is given by the following relations:

$$\varepsilon(\omega) = \varepsilon_\infty + \frac{A}{\omega_0^2 - \omega^2 - i\,\omega\,\Gamma(\omega)}$$

$$\Gamma(\omega) = \Gamma_0 \exp\left(-\left(\frac{1}{1+\sigma^2}\right)\left(\frac{\omega-\omega_0}{\Gamma_0}\right)^2 \right) \quad \text{(eq. 3)}$$

210 where A is the intensity of the oscillator, ω is the position, Γ is the amplitude and σ is called Gauss-Lorentz-switch. Like almost all fit parameters, it may vary between 0 and infinity. For $\sigma = 0$ a

Gaussian line shape is achieved, while large values of σ (larger than 5) lead to a Lorentzian. This latter feature is very advantageous because it allows to properly represent line shapes of multiple materials in either solid (crystal or amorphous) or liquid phase.

The use of the Kim oscillator is convenient, because it also requires a much less computational effort respect to other oscillators, like for example the Brendel oscillator (Brendel, 1990). This means that, if one has to work with many oscillators and combine them, using the Kim ones, it is in principle possible to save precious computational time and effort.

4.1 Optical response of an ideal dielectric: case of study

The optical response of real samples can be very complex because of the presence of multiple resonance peaks whose position and intensity may vary as a function of the orientation of the sample respect to the direction of propagation of the light. By orientation it is meant, both, the angle of incidence, i.e. the angle between the incident beam and the normal to the surface of the sample, and also the azimuthal angle, i.e. the angle between the optic axis of the sample and the plane of incidence. The plane of incidence contains the incident beam and its projection on the sample surface. Each resonance peak is linked to the vibration of one of the chemical bonds present in the crystal. Because of the particular crystal structure of the sample, each bond has a well-defined orientation in space and therefore reacts in a proper way to the polarized light. For this reason, the dependence of each resonance peak with sample orientation is particular and not necessarily identical to that of the other resonance peaks present in a given spectra. On top of that, in real samples the resonance peaks are not always well separated and may overlap to each other. As a result, the observed data is in general very rich and complex, which may lead to multiple ambiguities when it comes to build an optical model if some care is not taken. One of the most difficult aspects of building a parametric model for an anisotropic material is the creation of a correct function to represent the optical response of each one of the components of the dielectric tensor. A general dielectric tensor has six independent elements, but if this latter can be diagonalized, then, only three independent elements must be considered. Although the simplest function used for each tensor component includes a number of oscillators and a constant, the difficulty arises when it comes to assign the resonance peaks observed in the experimental data to the correct tensor elements. This assignment is not obvious, and the difficulty increases with the number of resonances observed in the data. In order to deal with this intricate situation we decided to profit the symmetry properties of the crystals. The symmetry of the crystal can be profited to use two rules of thumb, the first one is that the dichroism created by an infrared active vibration is maximal (minimal) when the polarization of the incident beam is parallel (perpendicular) to the

chemical bond at the origin of the vibration. The second rule of thumb is that any optical property must follow the symmetry of the crystal structure. In other words, the polarimetric properties must vary as a function of the orientation of the sample respect to the probing beam, but according to the symmetry properties defining the crystal structure.

To correctly interpret the data and the difference between isotropic and anisotropic samples, we studied first, the optical response of a uniform material with an ideal dielectric tensor. The ideal tensor is diagonal and each tensor element is represented by a parameterized mathematical function with one oscillator. The idea was to use the ideal material to simulate the dependence of the ellipsometric data with the orientation of the material to the incident beam and to observe how they depend on the presence (or absence) of oscillators in the dielectric tensor. Then, the result of these observations could be used, *in fine*, to stablish analogies with experimental data and therefore deduce the probable orientation of the bonds in the measured crystal. The optical model that we used to test the optical response of the ideal tensor was based on the following hypothesis:

- The tensor is diagonalizable and therefore the material can be either uniaxial or biaxial. This hypothesis is ideal to reproduce the optical response of cubic, orthorhombic, tetragonal, rhombohedral, or hexagonal crystals. Monoclinic and triclinic crystals, which are characterized by non-diagonalizable dielectric tensors, can be only approximately represented under this approach provided that the absorption is not too strong, i.e. the real part of the corresponding dielectric tensor elements remains positive.
- The sample is assumed to be a semi-infinite and homogeneous slab made of the material represented by the ideal dielectric tensor. The semi-infinite media implies that the only optical signal that is considered to the analysis is generated by light reflected by the uppermost surface (front face) of the sample. The influence of light coming from the back face of the sample, and therefore interference effects among light reflected by front and back face is ignored. This hypothesis, which is quite simplistic, is therefore compatible with the type of samples considered in this study because they only had a single face polished to an optical level. Light reaching the rear face of the samples, which was intentionally left unpolished is scattered and not collected by ellipsometer used in this study.
- The pseudo-dielectic function $<\varepsilon>$ is used together with the elements of the Mueller matrix to represent the optical response of the sample. The pseudo-dielectric function depends on the elllipsometric angles Ψ and Δ and the angle of incidence, θ_0, according to the following expression:

$$\langle \varepsilon \rangle = \sin(\theta_0)\left[1+\left(\frac{1-\tilde{\rho}}{1+\tilde{\rho}}\right)^2 \tan^2(\theta_0)\right] \text{ with } \tilde{\rho} = \tan(\psi)\exp(i\Delta) \qquad \text{(eq. 4)},$$

- *Strictu-senso*, when (eq. 3) is applied to the polarimetric data retrieved from an isotropic and semi-infinite sample, the pseudo-dielectric function represents the true dielectric function of it. When applied to an anisotropic sample, it provides the equivalent dielectric function of an isotropic material which would produce the same ellipsometric angles than the anisotropic material (Azzam and Bashara 1987). The pseudo-dielectric function of an isotropic material does not depend on either the angle of incidence or the azimuthal angle of illumination, however in general, the effective dielectric function of an anisotropic material does depend. This property of the pseudo-dielectric function can be used to identify the type of anisotropy of the considered material, reason why we include this observable in our analysis.

  Each oscillator used to represent a resonant absorption is modelled using the Kim oscillator formula (see for instance **Fig. 2**). The Kim oscillator equation allows the modification of the strength, position and spectral width of each resonance. Typical values for these parameters in the samples analyzed in this study are: ε_∞: 2.3, A (strength): 7x10^{-4}, ω_0 (spectral position): 0.15 eV, Γ_0 (spectral width): 0.003 eV, σ (Sigma): 0.1.
- Out of the resonance, the refractive index of the materials explored in this work is between 1.4 and 1.6. In consequence, typical values of the constant, ε_∞, are around 2.3. **Fig. 2** shows the typical dispersion of an oscillator with the parameters above-detailed. As can be seen, the oscillator describes a moderate to feeble absorption because the refractive index never goes below one, or, equivalently, the real part of the dielectric function is always positive.

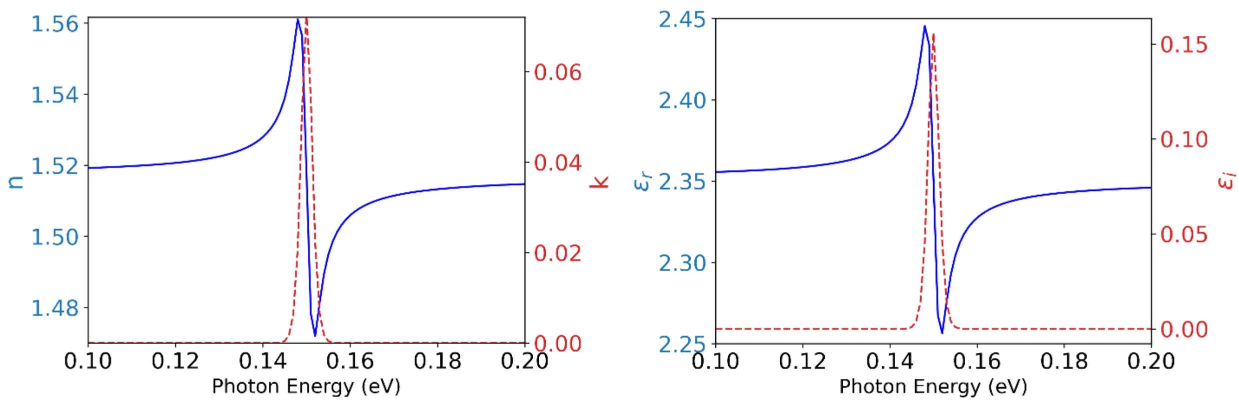

Fig. 2 – (left) Dispersion of the values of the refractive index, *n*, and the absorption coefficient, κ obtained with an oscillator described by the described in the text. (right) Same simulation, but using the real, ε_r and imaginary, ε_i, parts of the dielectric function as observables.

We studied the variations of the Mueller matrix elements and the retrieved peudo-dielectric dielectric function (real and imaginary parts, ε_r and ε_i, respectively). In the following section, a few measurement configurations are compared and discussed.

4.1.1 Anisotropic media: Influence of the angle of incidence

306 The case discussed here represents a very simple model of a biaxial material. A single oscillator is used for each one of the components of the dielectric tensor. The parameters used to build the dispersion of each component of the dielectric tensor are the following:

309
- ε_x : ε_∞=2.3, A=1x10^{-4}, **ω_0=0.18 eV**, Γ_0=0.003eV, σ=0.1.
- ε_y : ε_∞=2.3, A=1x10^{-4}, **ω_0=0.16 eV**, Γ_0=0.003eV, σ=0.1.
- ε_z : ε_∞=2.3, A=1x10^{-4}, **ω_0=0.14 eV**, Γ_0=0.003eV, σ=0.1.

312 To make things as simple as possible, the only difference among the parameters defining the oscillators is their respective spectral position. Moreover, the spectral position and width of the oscillators have been chosen to avoid any overlapping among them. In this way, the effect of each
315 oscillator appears in a well-defined spectral region, and therefore it is possible to study how each of them influence the spectral dependence of the Mueller matrix. In an anisotropic material, both the angle of incidence and the azimuthal angle may in principle have an effect on the Mueller matrix of
318 the sample. In our example we have chosen to vary first the angle of incidence choosing thee angles, one 10 degrees (46.6°) below the Brewster angle, θ_B, another one at θ_B (56.6°) and the third one 10 degrees (66.6°) above θ_B. These three angles have been chosen to show the interest of
321 making measurements close to the Brewster angle, and also to illustrate the interest of the study of the variation of the optical response with the angle of incidence to decide in which component of the dielectric function a given absorption should be. **Fig. 3** shows a selection of Mueller matrix
324 elements, and the pseudo-dielectric function, for the three angles of incidence above mentioned. The Mueller matrix elements not shown in Fig. 4 are either equal to a + or – sign to those shown, and therefore they do not carry any new information. For a full discussion about Mueller matrix
327 symmetry in ellipsometry see for instance (Arteaga, 2014). In the three cases illustrated in **Fig. 3**, the sample was oriented at an azimuth =0° which in practice means that the ***x*** component of the dielectric tensor is parallel to the plane of incidence, the ***s*** direction, and correspondingly, the ***y***
330 component of the dielectric tensor is perpendicular to the plane of incidence, the ***p*** direction.

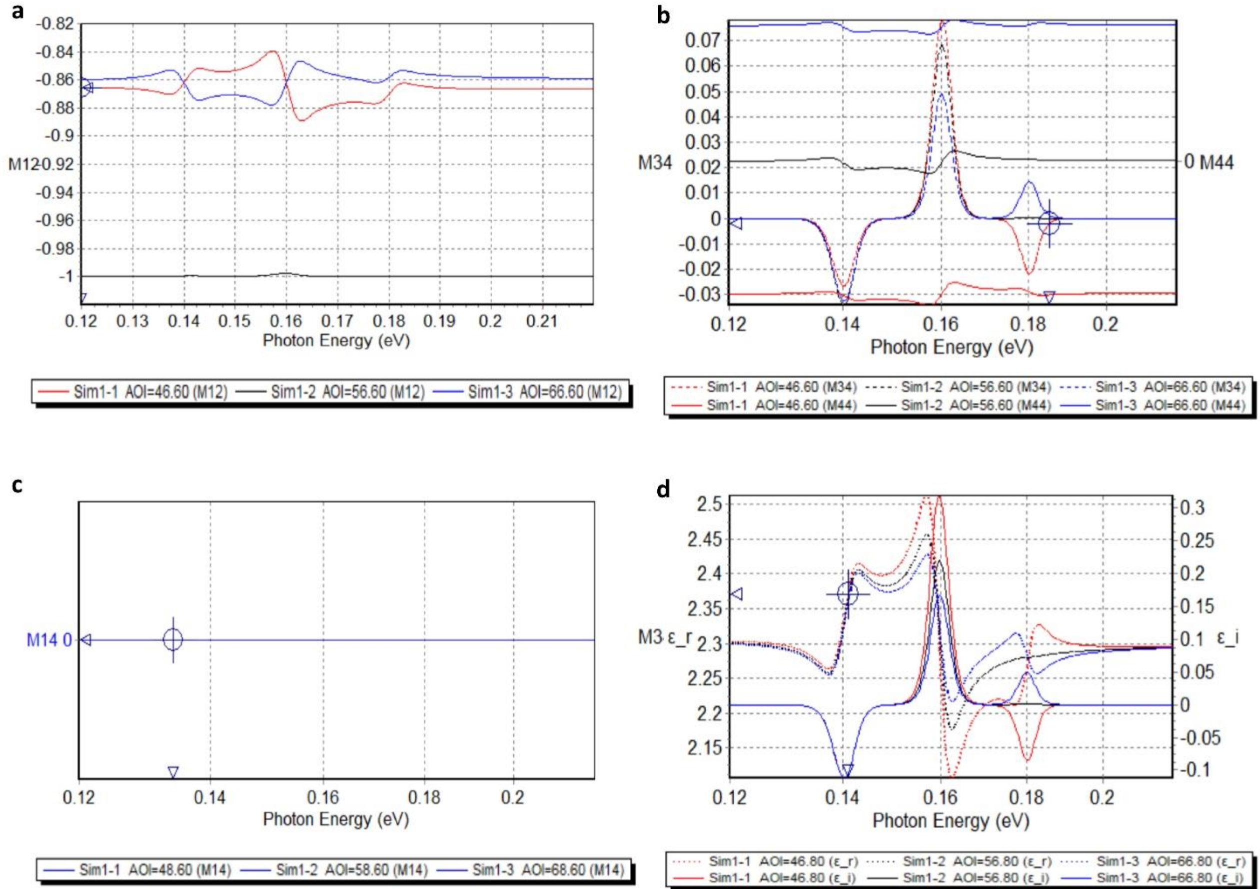

333 **Fig. 3** – a) Mueller matrix element M_{12} b) Mueller matrix elements M_{34} and M_{44} c) Mueller matrix element M_{14} d) Real, $<\varepsilon_r>$, and imaginary, $<\varepsilon_i>$, part of the pseudo-dielectric function.

From the simulated data in **Fig. 3**, it can be seen that the variation of the angle of incidence has an
336 impact on all the elements of the Mueller matrix and the dielectric function as well. However, the variation is not the same for three components of the dielectric tensor. These differences can give indices for the identification of patters in real data. In the Mueller matrix element M_{12}, the
339 absorptions appear as inflections, some of them with positive concavity and the others with negative concavity. The absorption in the ε_z component has a positive concavity below θ_B and at θ_B, however it transforms to a negative concavity above θ_B. The absorption in the ε_y component, *s*-polarized, has
342 a negative concavity below θ_B, and a positive concavity at θ_B and above it. The absorption in the ε_x component, *p*-polarized, is particular and illustrates the interest of measurements at θ_B or close of it; its concavity does not change with the angle of incidence, but disappears at θ_B. This property which
345 is in accordance with the definition of θ_B in a dielectric material, is useful in practice because it allows the identification of the absorptions which are mainly *s*-polarized from the others, and therefore facilitates the assignment to the ε_x or ε_y component of the dielectric tensor provided that
348 the azimuthal angle is known. The Mueller matrix element M_{34} also gives interesting clues to assign

absorptions to the corresponding component of the dielectric tensor. In the Mueller matrix element M_{34}, absorptions appear as peaks, whatever the angle of incidence; peaks are always negative for the ε_z component and positive for the *s*-polarized components (ε_y component in **Fig. 3**). On the contrary, peaks for p-polarized components (ε_x component in **Fig. 3**) are negative for incidence angles below θ_B, positive for angles above θ_B and null for at θ_B in accordance to the definition of Brewster angle. The Mueller matrix element M_{44} shows information analogous to that of the matrix element M_{12} concerning peaks. The interest of this element is that for spectral regions out of resonance, it becomes negative for angles of incidence below θ_B, positive for angles of incidence above θ_B, and null at θ_B. The element M_{44} is therefore a good indicator to decide whether measurements are done at an angle of incidence close enough to θ_B. Off-diagonal elements of the Mueller matrix such as M_{14} or M_{23} are null for azimuths 0° and 90°. The difference between absorption belonging to distinct components of the dielectric tensor is also well-visible in the dependence of the real and imaginary components of the pseudo-dielectric function with the angle of incidence. Absorptions in the component ε_z appear as negative peaks in the $\langle\varepsilon_i\rangle$ and as inflections with positive concavity in $\langle\varepsilon_r\rangle$. Interestingly, either $\langle\varepsilon_i\rangle$ or $\langle\varepsilon_r\rangle$ does not show any variation with the angle of incidence for absorptions in the ε_z component, which is a very good clue to identify absorptions belonging to the out of plane component. Spectral features belonging to a *s*-polarized absorption (ε_y component in **Fig. 3**) appear as an inflection with negative curvature in $\langle\varepsilon_r\rangle$ and positive peaks in $\langle\varepsilon_i\rangle$ the amplitude of the peaks or the inflections diminishes with an increasing angle of incidence, but there is no change of their respective sign. Finally, for p-polarized absorptions (εx component in Fig. 3) absorptions manifest as inflections with positive concavity below θ_B, negative concavity above θ_B, and they do not show any feature at θ_B. Correspondingly, the same absorptions appear as a negative peak for angles below θ_B, positive peaks for angles of incidence above θ_B, and they disappear at θ_B. The simulation shows that in the pseudo-dielectric representation each component of the dielectric tensor have a characteristic dependence, different to each other. For this reason, and despite of the fact that in general, the pseudo-dielectric function cannot be used to deduce with precision the value of the different components of the dielectric tensor, the use of this observable can help to properly assign oscillators to the different components of the dielectric tensor when it comes to build an optical model and to give an estimate of their respective strengths as well as for the average value of the constant ε_∞.

4.1.2 Anisotropic media: Influence of the azimuthal angle

The second parameter which can be scanned in a measurement run is the azimuth. In the following there is shown the effect of a rotation of the sample keeping an angle of incidence close to θ_B. The azimuthal angles chosen for the simulation are 0°, 45° and 90°. Simulations corresponding to azimuth 135° are not shown because they are redundant respect to simulations at an azimuth of 45°. In analogy to **Fig. 3**, the data shown in **Fig. 4** correspond to a selection of Mueller matrix elements and the pseudo-dielectric function.

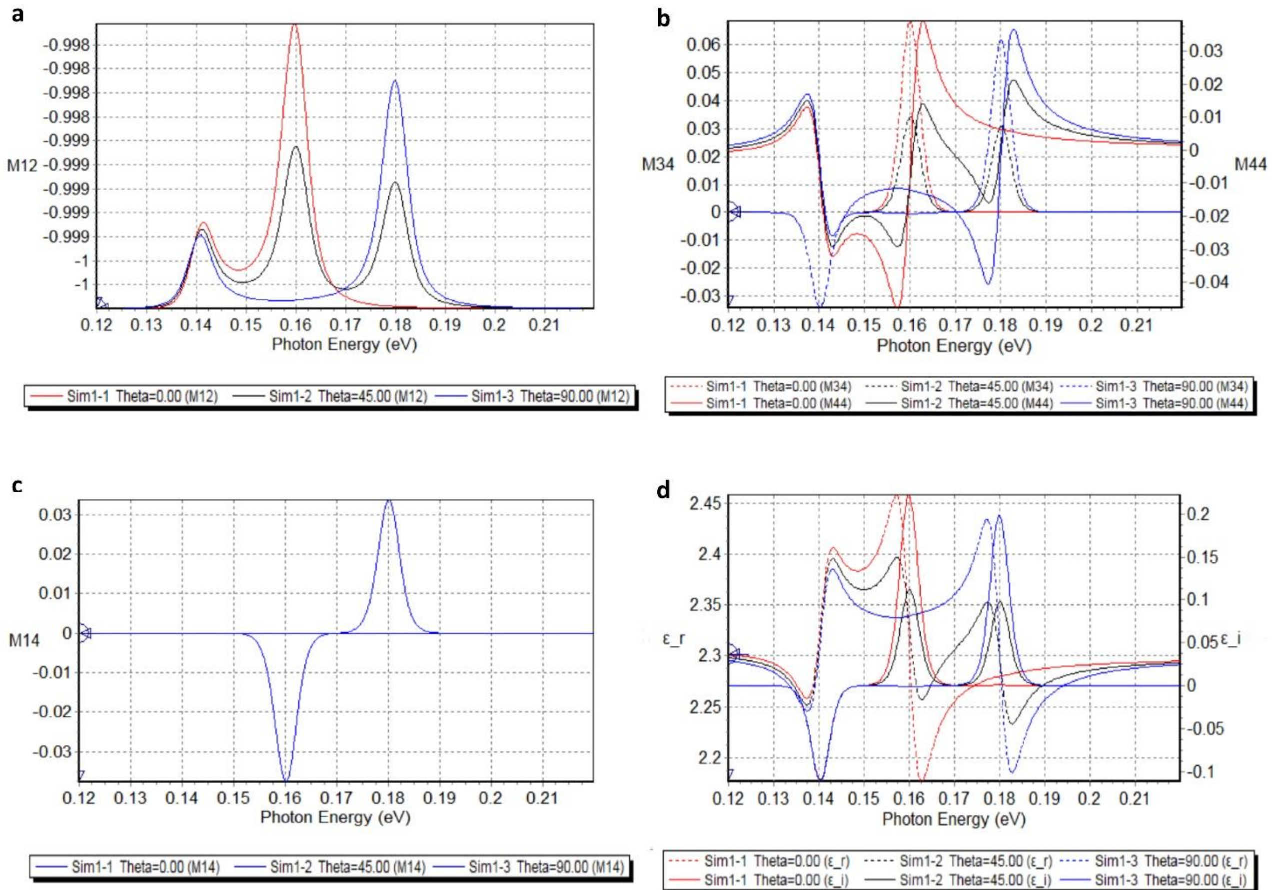

Fig. 4 – a) Element M_{12} b) Elements M_{34} and M_{44} c) Element M_{14} d) Real $\langle\varepsilon_r\rangle$and imaginary $\langle\varepsilon_i\rangle$ part of the pseudo-dielectric function.

Data for the azimuth 0° are the same shown in **Fig. 4**, for an angle of incidence equal to θ_B. Mueller matrix element M_{12} shows that rotating the sample from azimuth 0° to 90° transforms the ε_y component of the dielectric tensor in *p*-polarized whereas the component ε_x becomes *s*-polarized. In consequence, the only peaks which are visible in the M_{12} at azimuth 90° correspond to the ones in the ε_z (out of plane) and ε_x (*s*-polarized), while at azimuth, 0° the visible peaks are those due to the ε_z and the ε_y components of the dielectric tensor. Since the features due to ε_z remain unchanged, a comparison of data at azimuths 90° and 0° is a good way to identify features to the ε_z component (the unchanged part), the features due to the ε_x component (disappear or get minimized at azimuth

0°) and the features due to the ε_y component (disappear or minimized at azimuth 90°). Mueller matrix element M_{14} is only sensitive to the in plane components, ε_x and ε_y, of the dielectric tensor. Interestingly, the spectral features related to absorption appear as peaks. When the sample is turned to an azimuth of 45°, absorptions in the ε_y component appear as negative peaks while contributions of the ε_x component appear as positive peaks. Rotating the sample to 135° (not shown in the figure for clarity) will change the sign of the peaks, but does not bring any new information respect to the orientation at 45°. Mueller matrix element M_{14} is thus very important to discriminate between contributions due to ε_x from those due to ε_y. The information that can be retrieved from the analysis of either the pair of elements M_{32} and M_{44}, or, the real and imaginary parts of the pseudo-dielectric function is quite similar. Contributions from the out of plane component, ε_z, of the dielectric tensor appear as a negative peak and an inflection with a positive concavity in $\langle\varepsilon_i\rangle$ and $\langle\varepsilon_r\rangle$ respectively. Contributions due to the out of plane component remain unchanged when the sample is rotated. Comparing measures taken at azimuth 0° and 90° allow to get information about the contribution of the in plane components ε_x and ε_y, because at 0° the contributions due to the ε_x component (*p*-polarized at azimuth = 0°) are minimized while at azimuth 90° the contribution of the ε_y component (*p*-polarized at azimuth = 90°) are in turn minimized.

The previous simulation shows the importance of taking data at different angles of incidence and azimuthal angles when to characterize anisotropic materials to facilitate the task of building appropriate optical models.

4.2 Modelling of the data obtained for the gypsum sample

Starting from the experimental data, an anisotropic biaxial material was built with three different dielectric functions corresponding to each one of the diagonal components of the dielectric tensor, ε_x, ε_y and ε_z. Each dielectric function is made of a sum of Kim oscillators as in (Eq. 3). Following the general principles illustrated in the previous section, the parameters of the oscillators in the dielectric functions were determined on the basis of the positions and relative intensities of the peaks observed in experimental data measured at different azimuths. For the optical model, a flat semi-infinite medium was assumed. The Mueller matrices and pseudo-dielectric functions generated with the optical model were compared to the experimental data and then the parameters of the oscillators were fitted. Although in previous section it is shown the interest of using multiple angles of incidence to orient the construction of the theoretical dielectric tensor model, in the present study, due to the quality of samples used, it was not possible to do such type of measurements, reason why only measurements done at different azimuthal orientations were used. In order to simultaneously take into account the information provided by measurements at different

azimuths, a multi-model, capable of handling multiple data sets is used to simulate spectral Mueller
432 matrices and to fit them to the corresponding experimental measurements. The best fitted
parameters allowed the extraction of the optical constants of the material.

5. Results

435 While performing our experiments, it was observed that, sample preparation, measurements with an
ellipsometric approach, and data modeling must be done carefully. The sample preparation
procedure described in section 2 has been refined after several tests. It has been observed that for
438 raw minerals with non-polished surfaces, light was highly scattered, therefore almost no light
reached the detector because the aperture of the instrument is quite small, (just a tenth of a degree).
For double-polished samples, back-face contributions give non-coherent reflections, which are very
441 difficult to take into account when it comes to build a parametric dielectric tensor. Finally, for
samples prepared as thin sections, embedded in a mixture of resin and hardener, some loss of signal
has been observed when the polishing protocol results in polished, but not planar surfaces. Samples
444 prepared in thin sections are a good solution thanks to the fact that in most cases, the portion of the
sample that is embedded in the polymer is not flat and therefore scatters light away from the
specular direction, which avoids the reflection from the back surface. Despite of the net advantage
447 two problems were still present: i) the samples, although being polished one face, scatter a large
amount of the light which reduces the signal level and increases the noise in the final data; ii) the
two faces of the polymer holder in which the polymers were embedded, were non-parallel, the latter
450 was a problem when the azimuth was changed because the beam wandered and went out of the
detector easily. In such cases it was necessary to carefully tilt the sample-holder to realign the beam
trying, at the same time to not change the angle of incidence.
453 For the sake of illustration, an illustrative example of some of the data measured is shown in **Fig. 5**
together with the best fitted simulations obtained with the optical model.

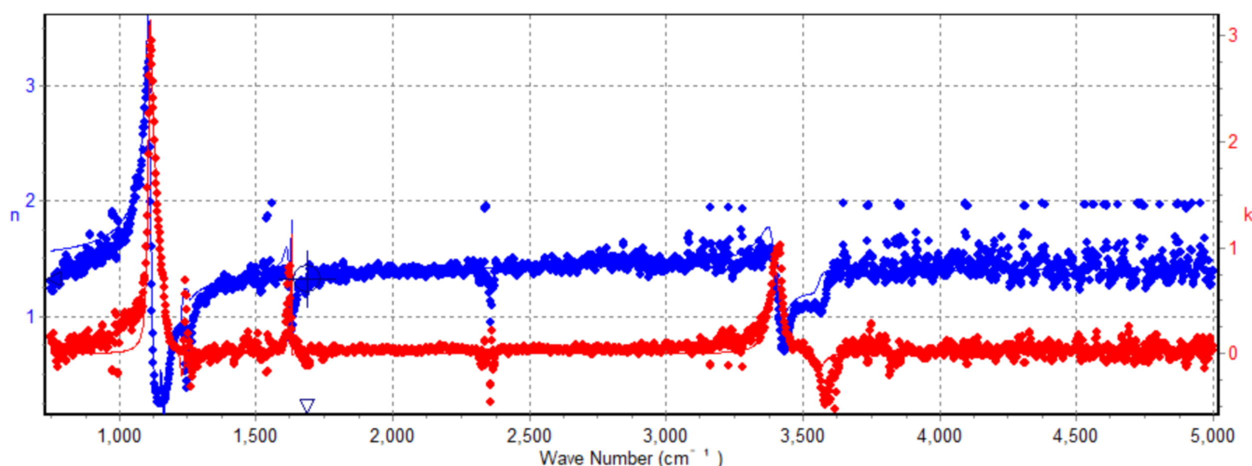

456 **Fig. 5** – Fit between experimental and theoretical data obtained from the gypsum sample.

For the gypsum sample, it has been possible to obtain a complete characterization of the optical constants for the three tensor components ε_x, ε_y and ε_z. The corresponding values, in the n, k
459 representation, are shown in **Fig. 6** to facilitate comparison with data found in the literature for gypsum, in particular for the values found by Long *et al*. (1993). Long *et al*. (1993) measured two crystalline samples of gypsum cut such that one plane was parallel to two axes forming the
462 monoclinic plane and the other was parallel to the third axis, allowing data to be acquired with the electric field parallel to each axis. Those data were treated in the framework of the dispersive analysis theory to obtain the dispersion of the different components of the dielectric tensor.

465 In gypsum, the crystallographic axes are defined by the following parameters. a = 5.679(5) Å, b = 15.202(14) Å, c = 6.522(6) Å, β = 118.43(4)°, and Z = 4 according to Pedersen, 1982. The ideal chemical formula of gypsum is $CaSO_4{\cdot}2H_2O$; and the crystal has a stratified structure, with the
468 layers lying along the crystallographic plane (010). Two layers of sulfate ions are bound together by calcium to form a robust double sheet. The double layers are linked together by sheets of water molecules. Each calcium ion is eight coordinated, six of these links are to oxygen atoms belonging
471 to sulfate atoms, and the remaining two links are to two oxygen atoms belonging to water molecules. The monoclinic plane in gypsum intercepts axes a, and c, while the axis b is mutually perpendicular to a, and c. In the measurements performed in this work samples were cut and
474 polished along the facile cleavage faces which are parallel to the crystallographic plane (010) (Pedersen, 1982, Antony, 1990), therefore the b axis was perpendicularly oriented to the surface of the samples, and it was collinear to the z direction of the reference frame used to define the
477 dielectric function. Accordingly, the crystallographic axis c coincided with the y direction of the same reference frame and laid on the sample surface. The crystallographic axis, a pointed towards the interior of the sample, and its projection to the sample surface, was parallel to the axis x of the
480 reference frame. As it can be seen in the results shown in **Fig. 6**, the optical response of gypsum in the measured spectral range is dominated by three non-overlapping spectral features situated at around 1100 cm^{-1}, 1629 cm^{-1} and 3500 cm^{-1}. The assignment of these features to particular vibration
483 modes is well known in the literature, see for instance Bishop, 2014, Seidl, 1968 or Haas, 1956; for more details. The feature at 1100 cm^{-1} is attributed to stretching vibrations of the O-P-O bonds in the phosphate units in the gypsum crystal. The unit cell of gypsum includes different phosphate
486 tetrahedra which are oriented along different directions in space, reason why the spectral feature corresponding to the O-P-O stretching has an influence on the three components of the dielectric tensor. Water molecules are preferentially oriented parallel to a plane which contains the
489 crystallographic axes b and c (Haas, 1956, Seidl, 1968). For this reason, the spectral features around

1629 cm^{-1} and 3500 cm^{-1} related to water vibrations show contributions to the ε_y and the ε_z components of the dielectric tensor only.

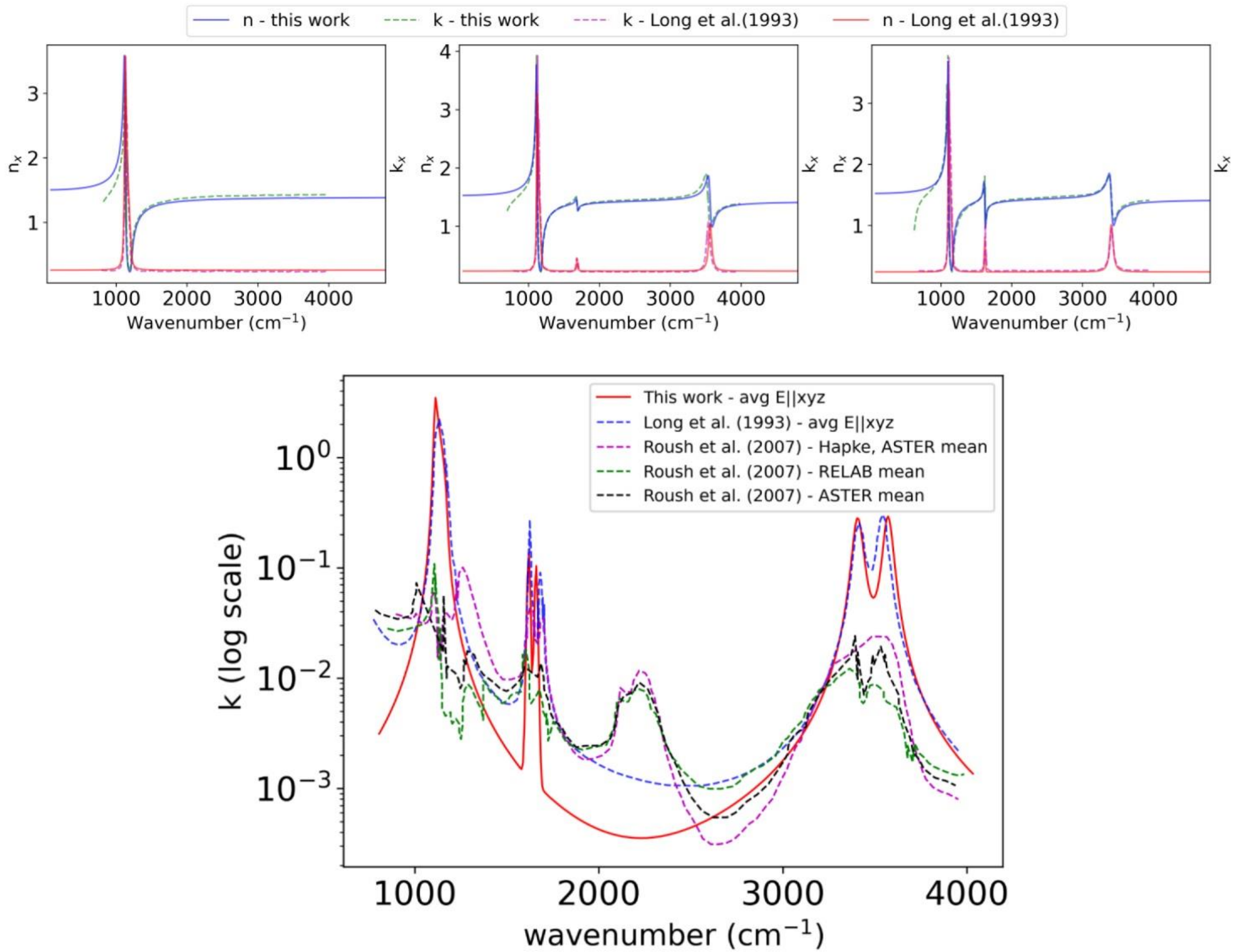

Fig. 6 – Up) Comparison between the optical constants obtained for the gypsum sample (M14) in the different three configurations: E||x, E||y and E||z in this work and those obtained by Long et al. (1993) - **Bottom)** Comparison between k obtained in this work and in the work of Long et al. (1993) and Roush et al. (2007).

As can be seen, in overall, the data taken from the literature are in good agreement with the results of the present work. Despite of the good agreement between results, a small discrepancy appears between data of this work and the literature data in the spectral windows around 1650 cm^{-1} and 3500 cm^{-1}, which the different vibration modes of water. The strength of infrared absorption in the latter spectral window depends of the hydration level of the sample, which may be affected by the origin, the history and the preparation of the studied specimen, and therefore may change from sample to sample. The broad absorption peak around 2300 cm^{-1} in the data from Roush *et al*, can be attributed to combinations of bands due to stretching vibrations of the phosphate group with the bending modes of water molecules (Hass, 1956). The absorption due to band combination is

generally not intense, and is more easily observed in transmission than in reflection measurements,
507 reason why the band is not present neither in Long *et al*. or in the present study data. It is important, however, to remind that all samples used in the present work and by other authors come from natural occurring mineral deposits, there is no a standardized material, and variations from sample
510 to sample are likely to happen.

Summarizing, it can be said that the ellipsometric method presented in this work allow for the determination of the dispersion of the three components of the dielectric tensor. Moreover, the
513 overall agreement between the optical constants obtained in this work and those discussed in the literature validates the ellipsometric method, and the data treatment protocol discussed in this work.

5.2 Results from reflectance measurements

516 The FTIR micro-Spectrometer was used to map the surface and to obtain a series of different spectra which created a sort of spectral microcartography of the gypsum sample. In this way, it was possible to evaluate effect of inclusions in the optical response of the samples used in this work .
519 Representative examples of these measurements are shown in **Fig. 7**. In which it is possible to see a microphotography taken at low magnification (**Fig. 7a**) in the visible, took with an auxiliary camera installed in the micro-spectrometer. In the selected area it is possible to see the surface of gypsum in
522 light gray and one inclusion in dark gray. The three other images (**Fig. 7b-d**) correspond to three areas in **Fig. 7a** imaged with higher magnification. **Area 1** and **Area 3** show very similar spectra, which indeed overlap and shown in **Fig. 7e**. Those regions can be considered as representative of
525 the majority of the sample surface. **Area 2** shows a quite different spectrum which is closer to that of a silicate than to that of gypsum. The spectrum of **Area 2** show a peak located at 1150 cm^{-1} (8.6 μm), and much less intense than the peak of gypsum at 1100 cm^{-1} related to phosphate absorption
528 present in **Area 1** and **Area 3**. As can be seen in the image of **Area 2,** the inclusions show a rougher surface than that of **Area 1** and **Area 3**, therefore the scattering level may be much more important, which explains why the signal level from regions similar to **Area 2** is less intense. Putting together
531 the fact that the signal level coming from inclusions is less intense than that of gypsum and the fact that the portion of the sample covered by inclusions was marginal compared to that of gypsum explain why the eventual inclusions present in the sample did not show a noticeable effect neither in
534 the ellipsometric measurements or the optical constants of gypsum derived from them.

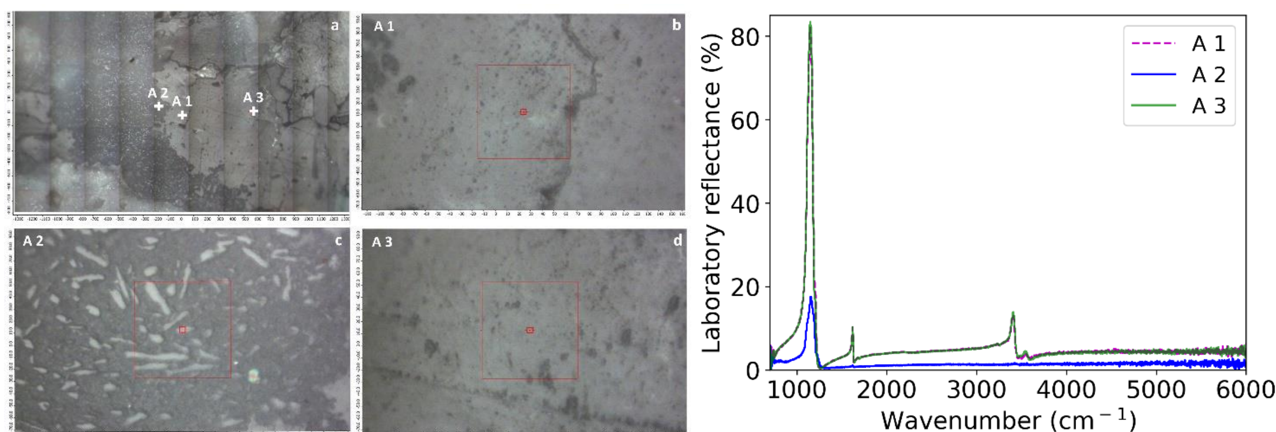

537 **Fig. 7** –Left - a) global image of the surface of the sample M14 analyzed at the FTIR MicroSpectrometer three white crosses indicates Area 1, Area 2 and Area 3 (A1, A2, A3), where the spectra were acquired. b) zoom of Area 1; c) zoom of Area 2; d) zoom of Area 3; Right - spectra 540 acquired from the three different areas of the sample surface.

6. Discussion and Conclusion

In this work, an experimental approach based on spectroscopic Mueller ellipsometric measurements 543 has been used on gypsum as an example of the validity of this technique for the determination of optical constants of planetary analog samples. Although ellipsometric measurements for materials characterization are current in materials science and the semiconductor domains, this is the first 546 time that the method is proposed to characterize planetary analog samples for the astronomical community. Keeping the latter on mind, in this paper a discussion is added to illustrate with a simple model the optical response an anisotropic material when it is studied with an ellipsometric 549 approach. To this end, it has been shown the interest of performing, when possible, measurements at different angles of incidence and azimuths, in order to highlight the contribution of each one of the components of the dielectric tensor of the sample under study. Moreover, a discussion is added 552 to illustrate the use of the information that could be retrieved from measurements to build an optical model of the dielectric tensor, which in turn has to be used to model the experimental data. Working with real minerals required a careful study of the sample preparation method in order to get samples 555 in a way that could be analyzed with the ellipsometric approach. In that way it was necessary to deal with some aspects related to the time consumed by the measurements, the difficulties in sample alignment, and, the quite complex data modeling for anisotropic samples. The optical constants of 558 gypsum obtained in this study in the MIR spectral region using the spectro ellipsometric method compare well with data obtained by other authors, which validates the approach. It is important to remind here that the optical model used in this study is an approximation for monoclinic and

triclinic crystalline materials, while it is exact for other crystals. Since a vast majority of clay materials and other analogs of Mars surface are either triclinic or monoclinic, in the near future, a more accurate model, including non-diagonalizable tensors, and based in the dispersion theory approach is going to be used to improve the accuracy of results.

In this perspective, a near future goal will be to optimize the measurement protocol, for instance, to prepare the sample in a way in that it will possible to know in advance the crystal orientation. Moreover, the technical configuration of the ellipsometer will be also improved to be able to perform measurements at multiple angles of incidence and at multiple azimuths to get the most from the samples as discussed in this paper. All the above optimizations will surely allow for the extension of the experiments to a wide range of planetary analogues and other materials of astrophysical interest.

Acknowledgements

This project was founded by NASA-JPL under grant agreement n° KM-2691-947266

References

Bibring J.P. et al.: 2006, Global Mineralogical and Aqueous Mars History Derived from OMEGA/Mars Express Data, Science, 312, 400.

Brendel R.: 1990, An infrared dielectric function model for amorphous solids, Journal of Applied Physics, 71, 587.

Ehlmann B.L. and Edwards S.E.: 2014, Mineralogy of the Martian Surface, Ann. Rev. Earth Planet. Sci., 42, 291.

Garcia-Caurel E. et al.: 2015, A mid-infrared Mueller ellipsometer with pseudo-achromatic optical elements, Applied Optics, 54, 2776-2785.

Kim C.C., Garland J.W., Abad H., Raccah P.M.: 1992, Modeling the optical dielectric function of semiconductors: Extension of the critical-point parabolic-band approximation, Phys. Rev. B 45, 11749-11767.

Long L.L. et al.: 1993, Optical properties of calcite and gypsum in crystalline and powdered form in the infrared and far-infrared, Infrared Physics, 34, 191-201.

Marzo G.A. et al.: 2004, The optical constants of gypsum particles as analog of Martian sulfates, Advances in Space Research, 33, 2246-2251.

Poulet F. et al.: 2002, Comparison between the Shkuratov and Hapke Scattering Theories for Solid Planetary Surfaces: Application to the Surface Composition of Two Centaurs Icarus, Icarus, 160,
594 313-324.

Poulet F. et al.: 2005, Phyllosilicates on Mars and implications for early Martian climate. Nature 438, 623-627, doi :10.1038/nature04274.

597 Poulet F. et al.: 2014, Mineral abundances at the final four curiosity study sites and implications for their formation, Icarus, 231, 65-76.

Stack K.M., Milliken R.E.: 2015, Modeling near-infrared reflectance spectra of clay and sulfate
600 mixtures and implications for Mars, Icarus, 250, 332-356.

1. R.M.A Azzam, N.M. Bashara, Ellipsometry and Polarized Light (Elsevier, Amsterdam, 1987).

G. E. Jellison, "Data analysis for spectroscopic ellipsometry", Thin solid films, Vol. 234, pp. 416-
603 422 (1993)

O. Arteaga, "Useful Mueller matrix symmetries for ellipsometry", Thin Solid Films, Vol. 571, pp. 584-588 (2014)

606 B. F. Pedersen, "Neutron Diffraction Refinement of the Structure of Gypsum, $CaSO_4 \cdot 2H_2O$", Acta Crystalographica, Vol. B38, pp. 1074-1077 (1982).

J. W. Anthony, R. A. Bideaux, K. W. Bladh, M. C. Nichols in Handbook of Mineralogy, Mineral
609 Data Publishing, Tucson Arizona, USA, p. gypsum (1990).

J. L. Bishop, M. D. Lane, M. Darby Dyar, S. J. King, A. J. Brown, G. A. Swayze "Spectral properties of Ca-sulfates: Gypsum, bassanite, and anhydrite", American Mineralogist, Vol. 99 p.p.
612 2105-2115 (2014).

V. Seidl, , O. Knop , M. Falk, "Infrared studies of water in crystalline hydrates: gypsum, $CaSO_4 \cdot 2H_2O$", Can. J. Chem. Vol. 47, pp. 1361-1368 (1969)

615 M. Hass, G. B. B. M. Sutherland, "The infra-red spectrum and crystal structure of gypsum", Proc. Roy. Soc. London, Ser. A, Vol. 236, pp. 427 (1956).